Title

Numerical simulation of secondary atomization of an emulsion fuel droplet due to puffing: Dynamics of wall interaction of a sessile droplet and comparison with a free droplet

Author(s)

Daisuke Tanimoto, Junji Shinjo

Numerical simulation of secondary atomization of an emulsion fuel droplet due to puffing: dynamics of wall interaction of a sessile droplet and comparison with a free droplet

Daisuke Tanimoto[1] and Junji Shinjo[1*]

[1]Department of Mechanical, Electrical and Electronic Engineering, Shimane University

1060 Nishikawatsu, Matsue 690-8504 Japan

[*]E-mail: jshinjo@ecs.shimane-u.ac.jp

Abstract

Physical mechanisms of explosive boiling of an ethanol-in-decane emulsion droplet are investigated by numerical simulation. Vapor bubble growth due to explosive boiling leads to secondary breakup of the droplet. The ethanol mass ratio is chosen in the regime of puffing (vapor ejection and partial breakup), which is generally likely to occur for a fuel spray in a combustor. Using both free and sessile droplet configurations and varying the initial number of boiling bubbles and the depth of the bubble formation in the dispersed sub-droplets, the droplet breakup and vapor mixing processes are discussed. For both free and sessile configurations, the basic dynamics of puffing is the same. When the bubble depth is deeper in the sub-droplet, the bubble growth is eventually larger. When the number of bubbles is more, puffing occurs several times, or the bubbles coalesce leading to larger bubble size, larger breakup and enhanced vapor mixing. In the sessile droplet configuration, the vapor ejection dynamics is essentially similar, but particularly when puffing is strong, the droplet bounces from the wall, first pushed toward the wall by the ejected vapor and then pulled from the wall due to the repelling and recoiling motion. Under such a condition, the initially attached droplet finally detaches form the wall and returns into the ambient gas. This phenomenon may transiently influence the mixture formation in a combustor when a fuel spray collides with the combustor wall. The present study serves as a first step toward a goal of quantitatively evaluating the puffing/microexplosion effect on a real fuel turbulent spray in internal combustion engines as to how large it can contribute to improving combustion performance, and insights have been obtained for future modeling which is expected to fill the gap between the droplet-scale and spray-scale knowledge.

Keywords: Emulsion, Free droplet, Sessile droplet, Puffing, Wall Bouncing

1.   Introduction

For internal combustion engines, fuel efficiency and exhaust gas cleanliness have been critical issues over decades. Using biofuels is considered as one of the effective ways to reduce overall carbon dioxide (CO_2) emission [1-5]. Biofuels are typically used in a blended form with fossil fuels since the physical properties are slightly different and utilization in existing engine devices is strongly required. Emulsion is one form of blended fuel, which is composed of immiscible components such as oil and alcohol, and typically one component is dispersed as small sub-droplets in a parent droplet of the other continuous component with the help of a surfactant agent [6]. The physical properties of components, such as boiling point temperature, surface tension, viscosity, etc., are typically different and emulsion fuels exhibit particular fluid dynamic behavior when heated in a combustor. One interesting phenomenon is puffing or microexplosion, which is secondary atomization induced by explosive boiling of contained dispersed-phase sub-droplets [1,4-28]. When an emulsion droplet is heated, the difference in boiling point temperature leads to superheated sub-droplets and these metastable sub-droplets may explode abruptly due to some disturbances [29-32]. As a result of this explosive phenomenon, the parent emulsion droplet breaks up partially (typically termed as puffing) or entirely (termed as microexplosion), which can play an important role in enhancing spray atomization [1,4-28]. The essential physical mechanism of puffing and microexplosion is the same and the terminology is mostly defined by the degree of breakup due to boiling bubble growth inside. Enhanced secondary atomization due to puffing or microexplosion also leads to enhanced mixing of fuel vapor and air, which may improve the combustion efficiency and reduce the hydrocarbon residue. Oxygenated fuels such as ethanol enhance the oxidation of carbon and are thus considered to reduce the production of particulate matter (PM) under some operating conditions [33,34]. These positive characteristics of emulsion fuels have motivated the present study.

Due to the above benefits, numerous studies on the atomization, mixing and combustion characteristics of emulsion fuels have been conducted so far. Experimentally, several studies have focused on demonstrating the effectiveness of blended fuels in engine-scale devices [4,5,22-28]. It has been demonstrated that the overall performance could be improved in terms of emission characteristics. However, the performance assessment may be sometimes combustor-specific and detailed physical processes occurring inside the combustor are typically difficult to observe or measure quantitatively. Several experiments [26-28] have reported that the flame characteristics have been changed due to puffing/microexplosion, such as ignition, spray angle and spray penetration, but detailed quantitative impact of puffing/microexplosion on the whole spray combustion dynamics is still not well known. More fundamentally, droplet-scale emulsion fuel experiments have been also conducted to elucidate physical mechanisms in detail [6-15,18,19,21]. In these studies, puffing or microexplosion dynamics was observed and its impact on vapor/air mixing and combustion was discussed. Puffing or microexplosion affects the gaseous vapor/air mixture transiently in a non-uniform manner and thus affecting the combustion behavior. Detailed observations or measurements of the droplet internal structures were also conducted to identify the evolution process leading to puffing and microexplosion [7-15,18,19,21]. In these studies, typically, the droplet scale is set at O(1mm) to make the experimental setup easier and to enable detailed observations. In a realistic fuel spray, however, the size of droplets

is O(1-10μm) and therefore the knowledge obtained through such experimental studies should be carefully treated. Mikami *et al.* [35] theoretically discussed the occurrence probability of microexplosion and shown that smaller droplets may have a smaller probability and the key is the time necessary for the inception of vapor nucleation, which is strongly related to the temperature inside the droplet. Recently, an experimental study on real-scale droplets has been reported by Watanabe *et al.* [25], in which even small droplets (30-50μm) in a spray exhibit puffing behavior when they have undergone heating. The dominant mode was puffing rather than microexplosion. The combustion experiments mentioned above [26-28] reported that puffing/microexplosion was observed in the spray flame region. Avulapati *et al.* [18] also reported that a small secondary droplet of 80μm can explode when it passes a very high-temperature region across a flame. Therefore, it is expected that even small droplets can exhibit puffing (or microexplosion with a less probability) behavior in some regions in a real fuel spray. However, quantitative knowledge on such a spray is still limited [25].

Numerical simulation could also play a role in elucidating the puffing/microexplosion dynamics of an emulsion droplet. One advantage of numerical simulation is that three-dimensional (3D) transient data can be obtained for a real-scale droplet of O(1-10μm). Currently, however, numerical simulation studies are relatively fewer [16,17,20]. Shinjo *et al*. have conducted detailed numerical studies on boiling bubble growth and puffing/microexplosion dynamics under various conditions [16]. Convective heating under the combustor-relevant conditions for a 30μm emulsion droplet has been also studied [36], where it was confirmed that the internal liquid circulation induced by the gas flow makes the local liquid temperature non-uniform and high mostly in the rear half of the droplet, which indicates a larger possibility of local puffing rather than entire microexplosion for a small droplet in a spray. Shinjo *et al.* [17,20] also unveiled the multiple droplets interaction under convective and reactive conditions mimicking droplets in the periphery of a jet spray because droplets deep inside the densely populated spray region cannot be exposed to the hot ambient air [37] and puffing/microexplosion is unlikely. By these studies, the transient fluid dynamic behavior leading to secondary atomization has been clarified, which can be used to consider the dynamics of a realistic emulsion fuel spray. These studies, however, have not discussed the behavior of an emulsion droplet deposited on the wall. In modern internal combustion engines where high pressure injection is used, the injected spray may collide with the combustor (cylinder or piston) wall and droplets may interact with the wall. In a larger scale setup (~O(1mm)), some experimental data of emulsion droplet/wall interaction are available [6,11], but the behavior for a small-scale (~O(1-10μm)) droplet is still unknown. Therefore, it is worth investigating the dynamics of puffing/microexplosion of a real-scale small droplet initially attached to the wall.

The objective of the present study is to unveil the fluid dynamic mechanism of puffing-induced secondary atomization of a sessile emulsion droplet on the wall by numerical simulation. Cases for a free droplet will be also considered for comparison. The ambient gas conditions are set to mimic a combustion chamber of a diesel engine. Diesel-biodiesel-bioethanol mixture is basically considered, and the physical properties of decane are used for surrogate purposes. Therefore, ethanol is dispersed as sub-droplets inside a parent droplet of decane. To see the parametric trends, the number and position of sub-droplets are varied and also the number and position of initial boiling bubbles inside the ethanol

sub-droplets are varied. The growth rate during the onset of puffing and the subsequent droplet breakup characteristics are discussed. For the sessile droplet cases, the interaction between the puffing droplet and the wall is also discussed to obtain further insights into emulsion fuel dynamics in a combustor. Still, phenomena in a fuel spray is complicated and the effect of secondary atomization on the spray dynamics and turbulent mixing should be carefully examined in the future for a quantitative evaluation. This study is one of the key steps toward that goal.

This paper is organized as follows. Section 2 describes the numerical formulations. Section 3 explains the numerical setup. Section 4 presents the results and discussion mainly focusing on the sessile droplet dynamics, with some comparison with that of free droplet cases. Finally, concluding remarks are given in Section 5.

2. Numerical formulations

The present study directly resolves the droplet interface motion and the governing equations are the 3D Navier-Stokes equations given as

$$\frac{\partial \mathbf{f}}{\partial t} + (\mathbf{u} \cdot \nabla)\mathbf{f} = \mathbf{g}, \tag{1}$$

$$\mathbf{f} = (\rho, \ \mathbf{u}, \ T, \ Y_i, \ F_k), \tag{2}$$

$$\mathbf{g} = (-\rho \nabla \cdot \mathbf{u} + S_\rho, \ -\frac{\nabla p}{\rho} + \mathbf{Q_u} + \frac{\mathbf{F_s}}{\rho} + \mathbf{S_u}, \ -T\left(\frac{\partial p}{\partial T}\right)_\rho \frac{\nabla \cdot \mathbf{u}}{\rho c_v} + Q_T + S_T, \ Q_{Y_i}, \ S_{F,k}), \tag{3}$$

where ρ is density, $\mathbf{u}$ velocity, T temperature and Y_i species mass fraction. Species of decane, ethanol, oxygen and nitrogen are considered in this study [16,17]. F_k $(= F_1, \ F_2)$ represents the level-set function [38,39], where two interfaces (one between gas and liquid and the other between liquid decane and liquid ethanol) are solved in this study [16,17,20]. p is pressure and c_v the specific heat at constant volume. $\mathbf{Q_u}$ is the term for the Newtonian viscous force. $\mathbf{F_s}$ is the term for surface tension modeled by CSF (Continuum Surface Force) method [16,17,20,40] and will be defined later. Q_T represents heat conduction modeled by Fourier's law, heat transfer due to mass diffusion and the work done by viscous force. Q_{Y_i} is the term for mass diffusion modeled by Fick's law. S_* is the source terms due to phase change (boiling) and will be defined later.

The level-set function is a signed distance function, which is used to capture an interface [38,39]. In this study, $F_1 = 0$ represents the air/decane interface and $F_2 = 0$ represents the decane/ethanol interface [16,17,20]. These level-set functions are combined with the MARS (Multi-interface Advection and Reconstruction Solver) method [41], a kind of VOF (Volume of Fluid) method, to improve the mass conservation in the level-set method [16,17,20,42].

Surface tension is modeled as a volume force by the CSF method [40], given as

$$\mathbf{F_s} = \sigma \kappa \delta \mathbf{n}, \tag{4}$$

where σ is the surface tension coefficient, $\kappa = -\nabla \cdot \mathbf{n}$ is the local surface curvature, $\mathbf{n}$ is the surface normal unit vector and δ is the delta function to identify the surface.

Phase change (boiling and evaporation) is formulated as jump conditions at the interface. Since the emulsion composed of immiscible liquids is considered and the liquid/gas interfaces are fully resolved, phase change of each component locally occurs independently. Although evaporation of

4

decane is also considered, its effect is minor. Therefore, boiling of ethanol is the primary cause of droplet breakup dynamics. In the general form of phase change, the jump condition for heat is [16,17,39]

$$h_l \dot{\omega} = [\lambda \nabla T \cdot \mathbf{n}], \tag{5}$$

where h_l is the latent heat of evaporation, $\dot{\omega}$ is the evaporation rate, λ is the thermal conductivity. $[f]$ denotes the difference of a variable f between the liquid and gas phase at interface, i.e., $[f] = f_L - f_G$. The subscripts L and G represent liquid and gas, respectively. The velocity at the interface satisfies [16,17,39]

$$\dot{\omega} = \rho_L(\mathbf{u_S} - \mathbf{u_L}) \cdot \mathbf{n} = \rho_G(\mathbf{u_S} - \mathbf{u_G}) \cdot \mathbf{n} \tag{6}$$

where the surface velocity $\mathbf{u_S}$ is defined as the sum of the liquid velocity and the surface regression velocity, i.e., $\mathbf{u_S} = \mathbf{u_L} + \mathbf{s_L}$ and $\mathbf{s_L} = s_L \mathbf{n} = \dot{\omega}/\rho_L \cdot \mathbf{n}$. Therefore, the jump condition for the velocity is

$$\mathbf{u_G} - \mathbf{u_L} = -(\rho_G^{-1} - \rho_L^{-1})\dot{\omega}\mathbf{n}. \tag{7}$$

From the above jump conditions, the source terms for phase change in Eq. (3) are [16,17]

$$S_\rho = \rho(\rho_G^{-1} - \rho_L^{-1})\dot{\omega}\delta, \tag{8}$$

$$\mathbf{S_u} = (\rho_G^{-1} - \rho_L^{-1})\dot{\omega}\left(\frac{\dot{\omega}}{\rho}\right)\delta\mathbf{n}, \tag{9}$$

$$S_T = -\left(\frac{h_l}{\rho c_p}\right)\dot{\omega}\delta, \tag{10}$$

$$S_{F,k} = -|\nabla F_k|s_L, \tag{11}$$

where c_p is the specific heat at constant pressure.

The numerical code used is called MEX (MicroEXplosion) [16,17,20,36,43-45]. Eq. (1) is solved by CIP (Cubic Interpolated Pseudo-particle) method [46,47]. The CIP method enables accurate calculation with less numerical diffusion and oscillation. This code has been used for various multiphase problems such as droplet pinch-off [43], turbulent liquid spray atomization [43,44] and evaporating spray dynamics [45], and the capability has been well demonstrated. From [16], two relevant validation cases are reproduced to demonstrate the effectiveness of the present numerical method. Figure 1a shows the 3D non-linear droplet oscillation of an initially prolate spheroid of $a/b=3$, where a is the length of its semi-major axis and b is the length of its semi-minor axis. The time is non-dimensionalized by $\sqrt{\rho_L r^3/\sigma}$ where the liquid density is $\rho_L=700\text{kg/m}^3$, surface tension $\sigma=20\times10^{-3}\text{N/m}$, equivalent radius $r=3^{1/3}b=2.9\times10^{-4}\text{m}$, viscosity $\mu_L=635\times10^{-6}\text{Pa·s}$ and the droplet Reynolds number is 100. The result from the present code [16] and the published result from [48] are in good agreement. Therefore, the interface dynamics can be properly captured. Next, Fig. 1b shows the boiling bubble growth [16]. The detailed case settings can be found in [16]. For all the cases, the bubble growth is in agreement with the theoretical prediction of diffusion-controlled growth [49,50], which is the main bubble growth mode except at the very initial moment (denoted as inertia-controlled). In the simulation cases, some oscillations can be also seen and the oscillation periods are also in good agreement with the theory [16,51]. Therefore, bubble growth can be well capture by the present method. More direct validation cases relevant to the present study can be found in [16,17].
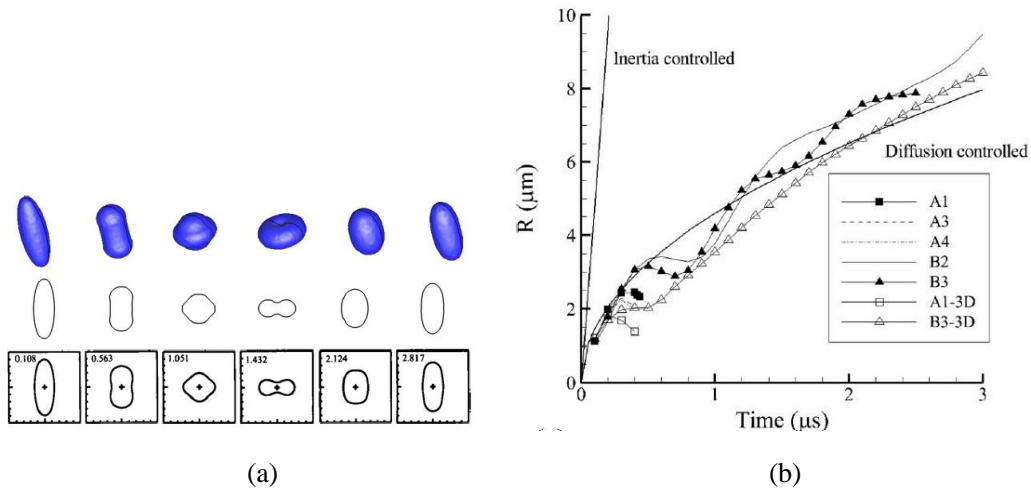
Fig. 1 Validation of the numerical method [16]. (a) 3D non-linear droplet oscillation. The upper line (3D overall view) and middle line (2D shape on the center plane) are from this code and the lower line represents the results from [48]. The time is 0.108, 0.563, 1.051, 1.432, 2.124 and 2.817, respectively. (b) Boiling bubble growth. Refer to [16] for detailed case descriptions. The images are reproduced from [16] under the Creative Commons BY license.

3. Case setup

The present study investigates the dynamics of explosive boiling of an emulsion droplet under conditions relevant to the combustion chamber in a diesel engine. Two configurations are considered: free droplet and sessile droplet. The free droplet configuration corresponds to a freely floating droplet in a spray and the sessile droplet configuration corresponds to a droplet attached to the wall after spray impingement. Common flow conditions are listed in Table 1. The ambient air pressure is set at 30atm and the ambient air temperature at 900K. For all the cases, the parent droplet diameter is set as D=30μm. This size is relatively large in a turbulent spray but this setting is intended because a larger droplet has more impact when puffing/microexplosion occurs in a spray [16,17]. The emulsion fuel components considered here are decane and ethanol (ethanol-in-decane) to mimic a Diesel, biodiesel and bioethanol mixture [17,18]. For the multi-species system of decane/ethanol/air, the above pressure still represents the subcritical pressure [52]. The mass ratio of ethanol is set at 11-16% in 3D (Cases S-4 and S-5) and 24-30% in 2D (other cases). It is experimentally reported that Diesel-ethanol mixture tends to be unstable and to separate when the mass percentage of ethanol becomes far higher beyond 10% (in 3D) [18]. Considering the easiness of fuel preparation in internal combustion engines, the above level of mass ratio is used in the present study. (Note that in 2D this percentage becomes relatively larger in appearance.) The experimentally observed mode for the above mixture ratio is typically puffing rather than microexplosion [18]. Therefore, puffing is mostly considered here. The boiling point temperature for ethanol is 460 K and the droplet temperature is initially set at 500 K, therefore the degree of superheat is 40 K, which is a realistic superheat degree for puffing [16,17]. The initial velocity is set as zero. Table 1 presents the physical properties as $\rho_{L,decane} = 650 \, \text{kg/m}^3$,

$\rho_{L,ethanol} = 800 \, \text{kg/m}^3$, $\mu_L = 1.6 \times 10^{-4} \text{Pa} \cdot \text{s}$ and $\sigma_L = 70.0 \times 10^{-3} \, \text{N/m}$. These values are slightly modulated from the real values to make the phenomenon slightly faster, but the essential dynamics can be captured [16,17]. Other properties such as heat of evaporation, heat capacities and others are temperature-dependent and retrieved from the database of NIST (National Institute of Standards and Technology) [53]. Since it is difficult to predict ethanol vapor nucleation deterministically, nucleation is initiated by giving a tiny vapor bubble whose initial diameter is 2.1μm inside the ethanol sub-droplet [16,17]. This setting means that the very initial bubble growth phase is skipped, but it has been demonstrated that this assumption would not cause any critically wrong behavior in the dynamics of puffing/microexplosion [16,17] (see Fig. 1b). It should be also stressed that it is not intended to consider only this specific combination of fuel type and flow conditions, but the fluid-dynamic results here can be applied to typical immiscible hydrocarbon-alcohol systems.

Parametric variations are mostly made in the 2D cases since it has been demonstrated that even 2D calculations can capture the parametric trend of puffing/microexplosion [16]. In addition, 3D cases are also conducted to fully capture the 3D effects. The grid spacing is 0.3μm in all cases. It has been demonstrated that this grid spacing is fine enough to capture the puffing dynamics for the size of the present droplets [16,17,20]. In 2D cases, the total number of grid points for the free droplet is 90,000 and for the sessile droplet is 48,000. In 3D cases, the total number of grid points for the sessile droplet is 14.4 million.

Table 1. Common conditions for all the cases

Droplet diameter D (μm)	Ambient pressure p (atm)	Ambient temperature T (K)	Parent droplet temperature (K)	Superheat degree of ethanol (K)
30 (F, S cases)	30	900	500	40
21.2 (WI cases)				

Decane density $\rho_{L,decane}$ (kg/m³)	Ethanol density $\rho_{L,ethanol}$ (kg/m³)	Liquid viscosity μ_L (Pa· s)	Surface tension (N/m)
650	800	1.6×10^{-4}	70.0×10^{-3}

(a) Free droplet cases

Figure 2 shows the schematic of droplet and bubble settings for the free droplet configuration. The calculation cases are listed in Table 2. These cases are set to mainly examine the effect of the number of boiling bubbles. One ethanol sub-droplet is placed inside the parent droplet. The initial ethanol sub-droplet diameter is set as 13.6μm. The ethanol droplet surface depth d is set to be 2.2μm and the distance of the vapor bubble center from the sub-droplet center R_b is 3.9μm in the +X direction in the baseline Case F-1. In Cases F-2 and F-3, the number of initial vapor bubbles is increased. As shown in Table 2, the bubbles are placed at the same distance of R_b=3.9μm from the sub-droplet center in

the ±X (Case F-2) and ±X and ±Y directions (Case F-3), respectively. The computational domain size is 90×90μm (3D×3D).
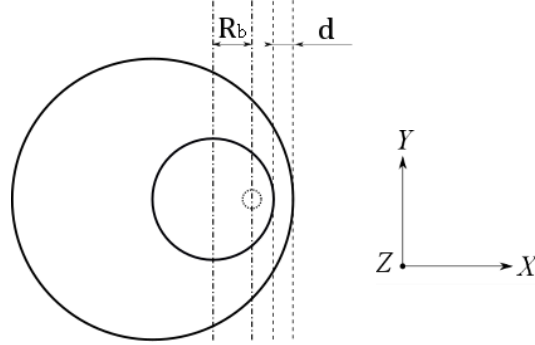
Fig. 2 Setup of sub-droplet and bubble for the free droplet configuration.

Table 2 Calculation cases for the free droplet configuration.

	d (μm)	R_b (μm)	Number and size of sub-droplets	Mass ratio of ethanol	Number of boiling bubbles
Case F-1 (2D)	2.2	3.9 in +X direction	1, 13.6μm	24%	1
Case F-2 (2D)	2.2	3.9 in ±X direction	1, 13.6μm	24%	2
Case F-3 (2D)	2.2	3.9 in ±X, ±Y direction	1, 13.6μm	24%	4

(b) Sessile droplet cases

Figure 3 shows the schematic of droplet and bubble settings for the sessile droplet configuration to investigate the interaction between the droplet and the wall. The calculation cases are listed in Table 3. The basic configuration is the same as that of the free droplet cases, and 3D cases are added. The number of ethanol sub-droplets is one for Cases S-1 to S-4 and four in Case S-5. The initial decane droplet diameter (contact diameter on the wall) D is set to be 30μm, and the initial decane droplet height H is 15μm. S-4 and S-5 are 3D cases. S-5 is to see the effect of the number of sub-droplets, and the sub-droplet size and position are slightly different to see the effect of more dispersed ethanol. The initial ethanol sub-droplet diameter is 10.8μm for Cases S-1 to S-4 and 7.6μm for Case S-5.

It has been reported that typically nucleation is likely to occur near the sub-droplet interface [29-32], but here a larger variation is given to see the dynamic effect of nucleation position. In Case S-1 and Case S-2, one bubble is placed in the vicinity of the ethanol droplet interface on the ambient air side (+Y) (Case S-1) and at the center of the ethanol sub-droplet (Case S-2), respectively. In Case S-3, two bubbles are placed in the ±X direction symmetrically. In Case S-4 (3D), four bubbles are placed in the ±X and ±Z directions symmetrically. In Case S-5 (3D), one bubble is placed at the center of each ethanol sub-droplet. The wall contact angle is set to be 120 degrees in all cases, which is to mimic the slightly hydrophobic condition often encountered in microexplosion experiments on the hot wall [6,54,55]. This setting of the statically fixed contact angle is to primarily focus on the droplet dynamics

due to bubble growth. Under some conditions, however, the wall contact angle may statically or even dynamically vary depending on the wall characteristics. This effect will be investigated in the future. The wall temperature is hypothetically set at 900K, but the heat transfer from the wall is not considered since the puffing dynamics is much faster. The computational domain size is $90\times48\mu m$ ($3D\times1.6D$) in 2D cases and $90\times90\times48\mu m$ ($3D\times3D\times1.6D$) in 3D cases.
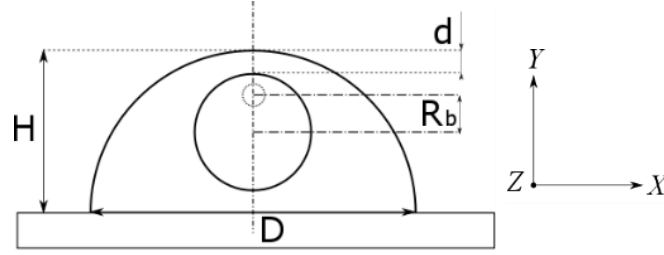
Fig. 3 Setup of sub-droplet and bubble for the sessile droplet configuration.

Table 3 Calculation cases for the sessile droplet configuration.

	d (μm)	R_b (μm)	Number and size of sub-droplets	Mass ratio of ethanol	Number of boiling bubbles
Case S-1 (2D)	2.2	3.3 in +Y direction	1, 10.8μm	30%	1
Case S-2 (2D)	2.2	0.0	1, 10.8μm	30%	1
Case S-3 (2D)	2.2	3.3 in ±X direction	1, 10.8μm	30%	2
Case S-4 (3D)	2.2	3.3 in ±X, ±Z direction	1, 10.8μm	11%	4
Case S-5 (3D)	2.2	0.0	4, 7.6μm	16%	4

(b-2) Wall impacting droplet cases (reference cases)

In order to discuss the wall bouncing behavior in 4.3, additional reference cases of wall impacting droplet are considered. The configuration is schematically shown in Fig. 4. An emulsion droplet with its initial downward velocity is placed 2μm above the wall and it will quickly hit the wall surface. The initial velocity U is varied between Cases WI-1/2 and WI-3/4, and the droplet Weber and Reynolds numbers, defined as $We = \rho_L DU^2/\sigma_L$ and $Re = \rho_L DU/\mu_L$ respectively, change accordingly. Here, the parent droplet diameter is $D=21.2\mu m$, which is to make the total volume the same as that of the sessile droplet (Cases S-1 to S-3), and the sub-droplet diameter is $D_{sub}=10.8\mu m$. Cases WI-1 and WI-3 are without puffing and Cases WI-2 and WI-4 are with puffing. One vapor bubble is placed at the center of the sub-droplet to initiate puffing. Table 4 summarizes the flow conditions. The computational domain size is $100\times40\mu m$ ($4.7D\times1.9D$). Other conditions are the same as those of the sessile droplet cases.
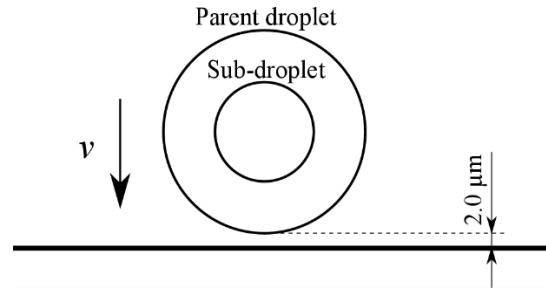
Fig. 4 Schematic of wall impacting cases. One sub-droplet is placed at the center.

Table 4 Reference calculation cases of wall impact.

	Impacting velocity (m/s)	Droplet Weber number	Droplet Reynolds number	Number and size of sub-droplets	Number of boiling bubbles
Case WI-1	5.0	4.9	431	1, 10.8μm	no puffing
Case WI-2	5.0	4.9	431	1, 10.8μm	1
Case WI-3	30.0	177	2584	1, 10.8μm	no puffing
Case WI-4	30.0	177	2584	1, 10.8μm	1

4. Results and discussion

4.1. Overall puffing dynamics of a free droplet

After boiling bubbles are initiated in the ethanol sub-droplet, these bubbles continue to grow due to explosive boiling, and subsequently the parent droplet surface ruptures and the ethanol vapor is ejected. Accordingly, part of the parent droplet would break up into smaller secondary fragments. Figure 5 shows the droplet shape and the ejected ethanol vapor distribution for Cases F-1, F-2 and F-3 at 1.0μs after all bubbles have ejected the vapor into the ambient air. In the droplet, the yellow part represents decane and the red part ethanol. The blue region in the gas phase shows the ethanol vapor mass fraction.

(a)   (b)
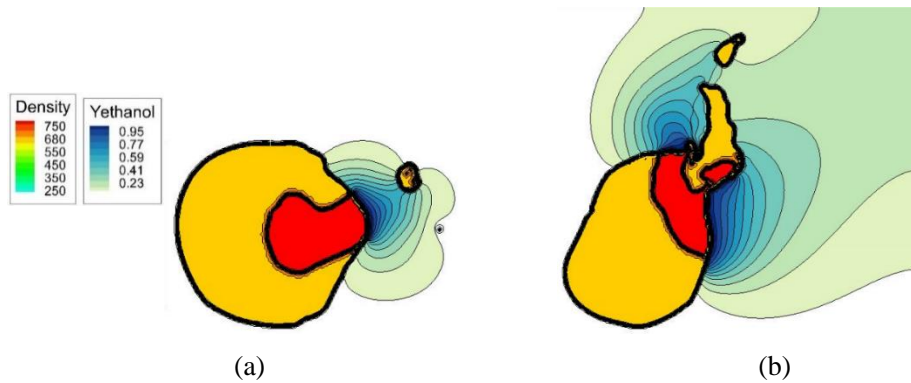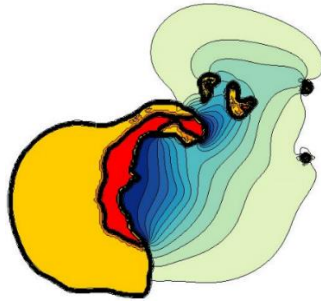
(c)

Fig. 5 Droplet shape and distribution of ethanol vapor mass fraction. (a) Case F-1 at t=2.7μs, (b) Case F-2 at t=7.4μs and (c) Case F-3 at t=3.6μs.

For the overall parent droplet breakup, the number of puffing events is one of the factors that determine the breakup intensity. Comparing Cases F-1 and F-3, Case F-3 has three more bubbles and the breakup is larger than Case F-1, as is evident in Fig. 5.

For each puffing event, the bubble size before rupture is also an important factor. Figure 6 shows the comparison of the elapsed time leading to puffing for each case. The vertical axis represents the time interval between each puffing event and the horizontal axis represents the sequential number of each puffing event (1 means the first puffing). As seen in Fig. 6, the elapsed time for the first puffing is almost comparable in all cases since the bubble closest to the parent droplet surface is placed at the same position. However, the elapsed time for the subsequent puffing in Case F-3 is shorter than that in Case F-2. This is due to the closer distance between each bubble in Case F-3, as shown in Fig. 7. Therefore, these bubbles tend to coalesce more easily and the interval of puffing becomes shorter, which makes each puffing event relatively less strong. With the longer bubble growth of the deeper bubble in Case F-2, the eventual puffing is stronger. Figure 8 shows the evolution of puffing for Cases F-2 and F-3. As is evident, each puffing occurs independently in Case F-2 and merging of puffing bubbles can be observed in Case F-3. These results are consistent with the reported results in [16].
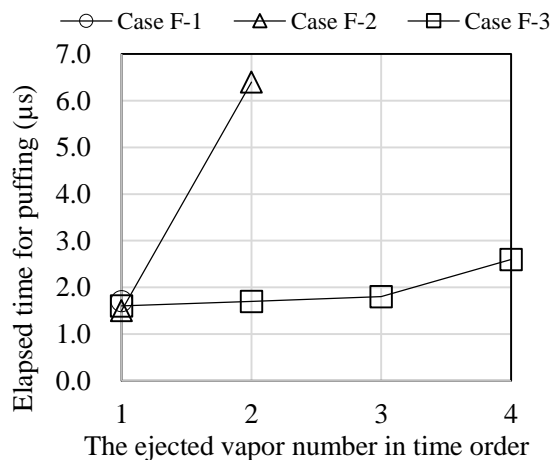
Fig. 6 Elapsed time for the occurrence of each puffing (μs) in the free droplet cases.

11
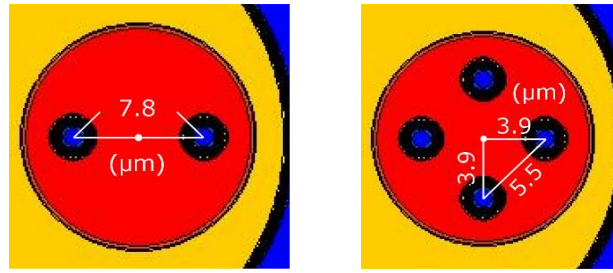
(a)   (b)

Fig. 7 The closest distance between bubbles. (a) Case F-2 and (b) Case F-3.
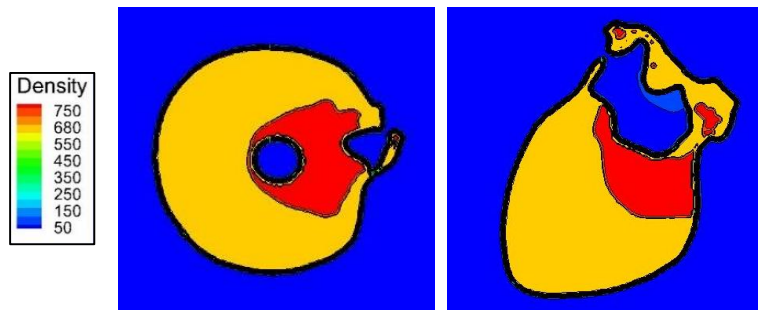
(a) Case F-2 at t=1.5μs (left) and t=6.4μs (right)
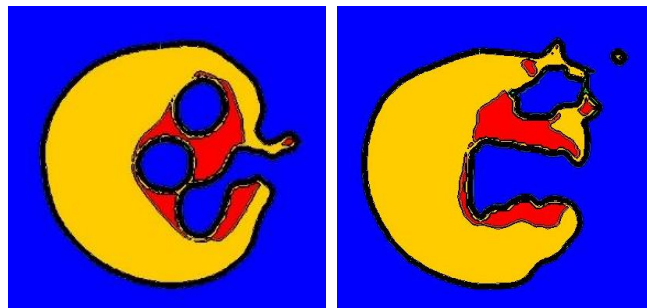
(b) Case F-3 at t=1.8μs (left) and t=2.6μs (right)

Fig. 8 Droplet shape at the instants of puffing. (a) Independent puffing in Case F-2 and (b) merged puffing in Case F-3.

4.2. Overall puffing dynamics of a sessile droplet on the wall

Figure 9 shows the droplet shape and the ejected ethanol vapor distribution for Cases S-1 to S-3 at 1.0μs after all bubbles have ejected the vapor into the ambient air. It is clear that the puffing and subsequent breakup behavior is essentially the same as that for the free droplet cases in 4.1. Explosive boiling initiated in the bubbles leads to bubble growth, rupture and ejection of the vapor.

(a) Case S-1 at t=2.2μs (b) Case S-2 at t=5.0μs
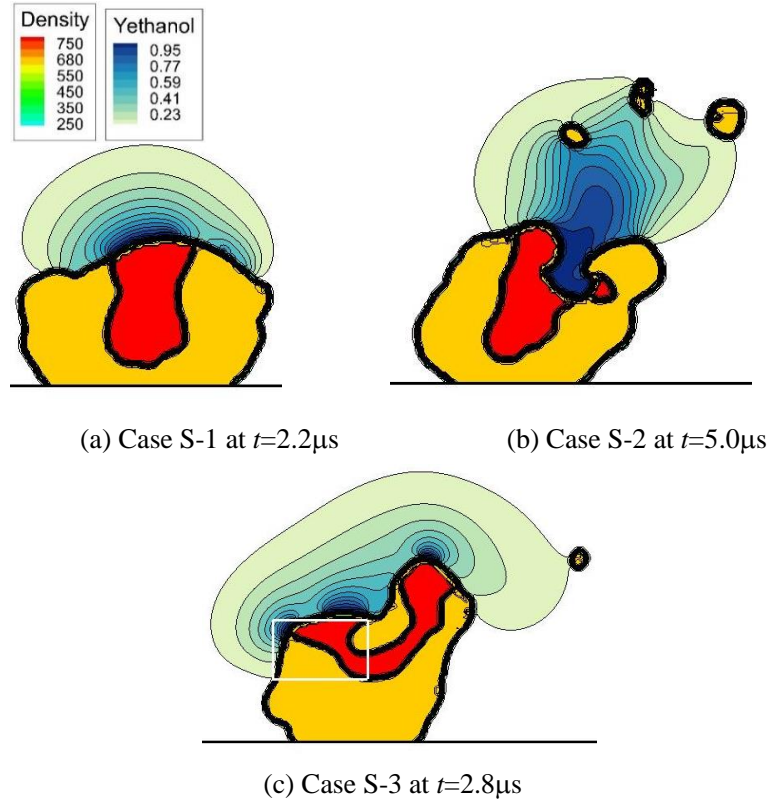
(c) Case S-3 at t=2.8μs

Fig. 9 Droplet shape and distribution of ethanol vapor mass fraction for the sessile droplet cases (2D). (a) Case S-1 at t=2.2μs, (b) Case S-2 at t=5.0μs and (c) Case S-3 at t=2.8μs. The 2D droplet coloring is the same as that in Fig. 5. The white rectangle in (c) will be later used for discussion in 4.3.

The elapsed time from bubble initiation to puffing is shown in Fig. 10a, which also indicates that as the depth of the bubble is deeper in the sub-droplet, the elapsed time for the puffing is longer. The size history of the bubbles in Fig. 10b indicates the longer growth means a larger bubble. As a result, comparing Cases S-1 and S-2, it is clear that in Case S-2 where the initial bubble position is deeper toward the center of the sub-droplet and the bubble is contained in the parent droplet until it becomes substantially large, the eventual breakup is larger. Comparing Cases S-1 and S-3, it is clear that in Case S-3 where the droplet has multiple bubbles although each bubble growth is similar to that in Case S-1, the droplet deformation becomes overall larger due to the combined effect of two bubbles, leading to larger breakup.
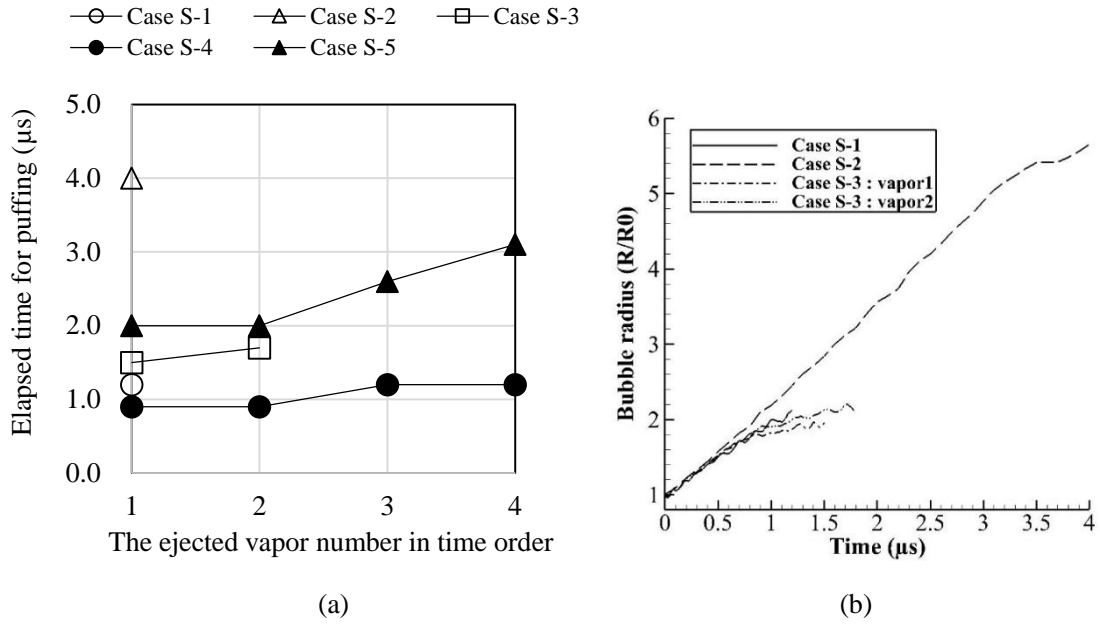
Fig. 10 Bubble growth behavior in the sessile droplet cases. (a) Elapsed time for the occurrence of each puffing (µs) and (b) temporal history of bubble size. R_0 is the initial bubble size and R is the effective radius calculated from the volume.

3D Cases S-4 (one sub-droplet and four bubbles close to the parent droplet surface) and S-5 (four sub-droplets with one bubble each at deep inside) in Fig. 11 indicate the similar behavior. Again, the droplet deformation is larger if the bubble growth is larger. In Case S-4, each vapor is ejected separately. This is because the bubble surface depth is small (1.05µm) and bubbles rupture before they grow large enough. In Case S-5, coalescence of sub-droplets and bubbles occur and the bubble size is larger as shown in Fig. 11 and the entire puffing is stronger.

Due to the wall, the breakup direction is limited and this may cause particular behavior of wall bouncing. In fact, bouncing is observed in Cases S-2, S-3 and S-5 where puffing is relatively stronger. This will be discussed later in 4.3.

(a-1) Case S-4 at t=2.2μs (bird's view)   (a-2) top view of Case S-4 at t=0.9μs and t=1.2μs

(b-1) Case S-5 at t=4.1μs (bird's view)

(b-2) top view of Case S-5 at t=1.5μs, t=2.0μs, t=2.6μs and t=3.1μs
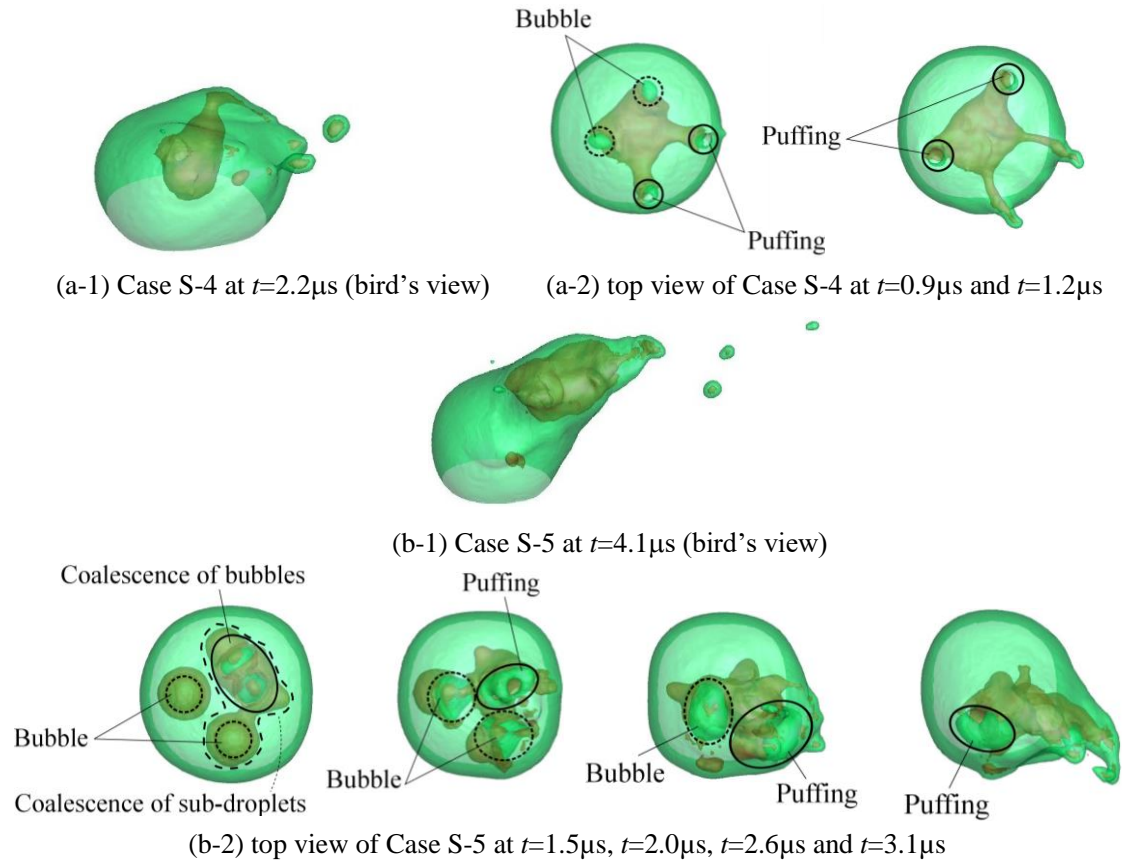
Fig. 11 Behavior of the vapor bubbles during puffing in 3D cases. (a) Case S-4. (b) Case S-5.

4.3 Puffing and wall bouncing

Figures 12 and 13 show the temporal evolution of wall bouncing cases of S-3 (2D) and S-5 (3D). In Fig. 13, the non-bouncing case of S-4 is also shown for reference. In Case S-3, initially at t=1.5μs and t=1.8μs, it can be seen that the two grown bubbles rupture and eject the vapor into the ambient air. This vapor ejection is toward the +Y (upper) direction and serves as a thrust force to push the parent droplet downward (in the –Y direction). Since the droplet motion in the –Y direction is restricted by the wall, the droplet starts to bounce back changing its shape. The concave surface shape after vapor ejection at t=2.0μs has changed to the convex shape at t=3.0μs and the droplet shape extends vertically. Finally, the entire droplet is detached from the wall around t=5.0μs. After detachment, the droplet tries to recover to a spherical (circular in 2D) shape with some shape oscillation. The behavior in 3D (Case S-5 in Fig. 13a) is similar. Note that in 3D, generation of a ligament from the droplet surface after puffing and subsequent secondary droplet pinch-off due to surface tension can be more clearly seen than in 2D cases [17-21] since the surface tension evaluation can be done properly in the two principal directions [43]. This ligament ejection is a result of the formation of the dynamically free portion of liquid with the outward velocity, due to the local liquid motion [56,57]. Once the liquid portion becomes free, it is eventually pinched-off as a ligament after the continuous outward motion.
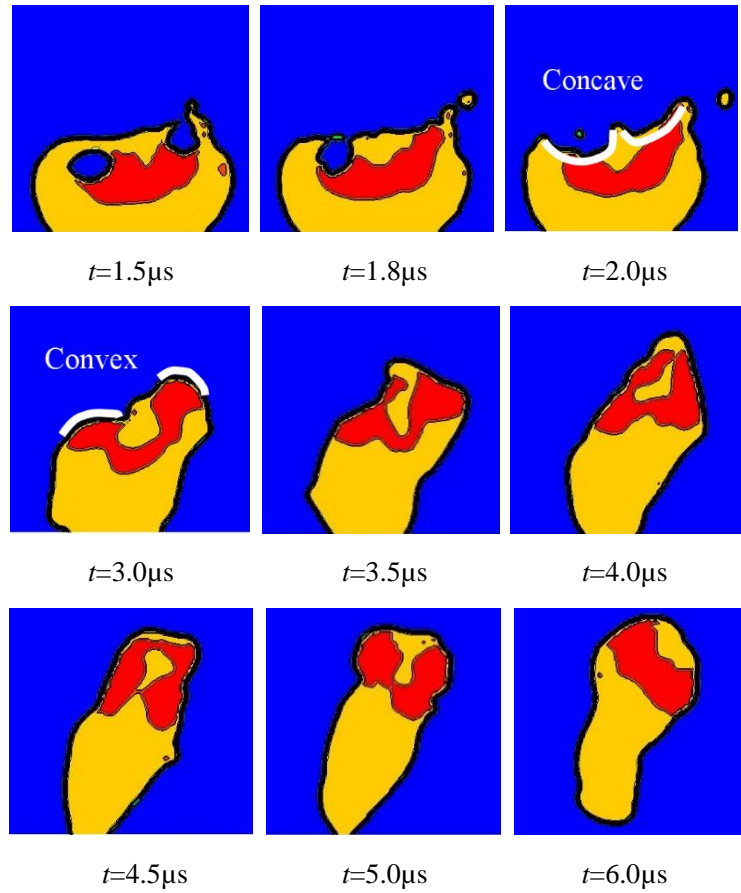
Fig. 12 Bouncing of droplet in Case S-3. The droplet coloring is the same as that in Fig. 8.
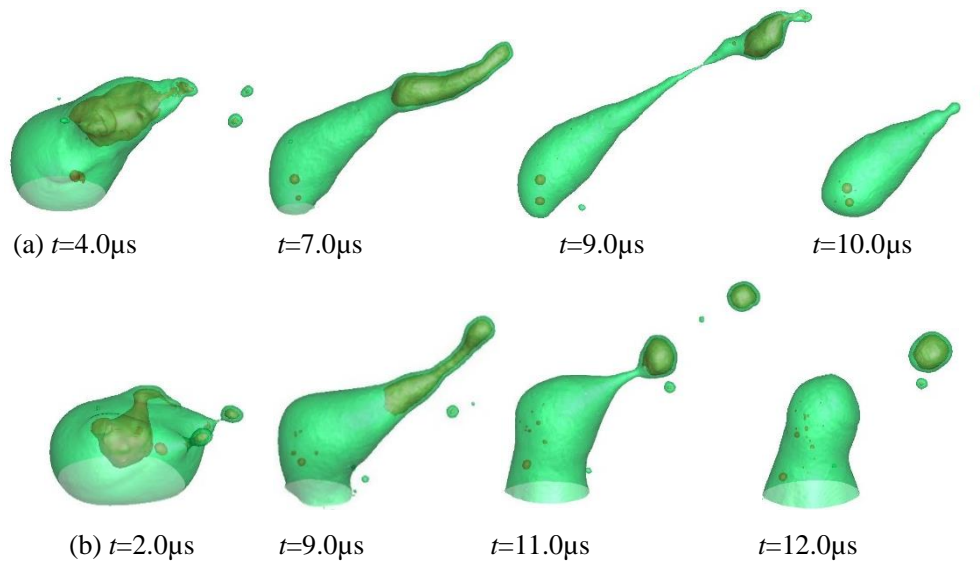
Fig. 13 3D droplet behavior with puffing. (a) Case S-5 (bouncing case) and (b) Case S-4 (non-bouncing case).

Figure 14 shows the evolution of the surface area including both the parent and secondary droplets. It is non-dimensionalized by the initial surface area of the parent emulsion droplet S_0. It is clear that the bouncing cases (S-2, S-3 and S-5) exhibit the larger magnitude in the surface area increase during puffing than the non-bouncing cases (S-1 and S-4). This is to indicate that the strength of puffing can be a factor to determine the bouncing behavior. Case S-3 is then further detailed to identify the motion leading to wall detachment.

(a)   (b)
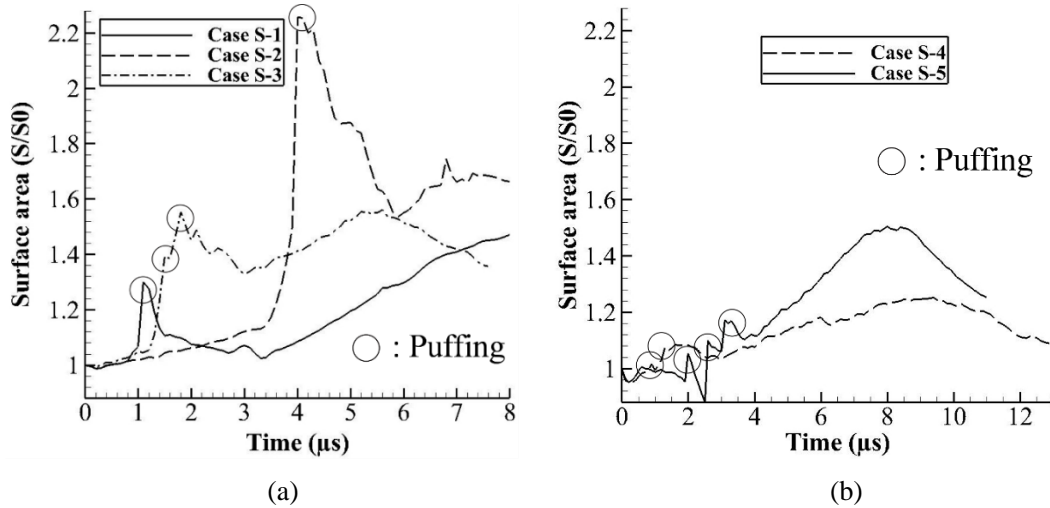
Fig. 14 Temporal evolution of droplet surface area. (a) Sessile droplet (2D) and (b) sessile droplet (3D).

The time history of the Y-direction mean velocity v of the parent droplet surface in Case S-3, averaged in the ejection area indicated by the white rectangle in Fig. 9c, is shown in Fig. 15a. The mean velocity v is initially stable around zero with small oscillations due to boiling bubble growth inside. After puffing it steeply becomes negative (pushed in the –Y direction) and quickly turns positive (rebound in the +Y direction). The shape transformation from concave to convex, shown in Fig. 12, corresponds to this period of time (2.0~3.0μs). The entire droplet velocity (velocity of the center of mass) in the +Y direction, shown in Fig. 15b, also indicates the same behavior of velocity increase in the +Y direction after puffing.
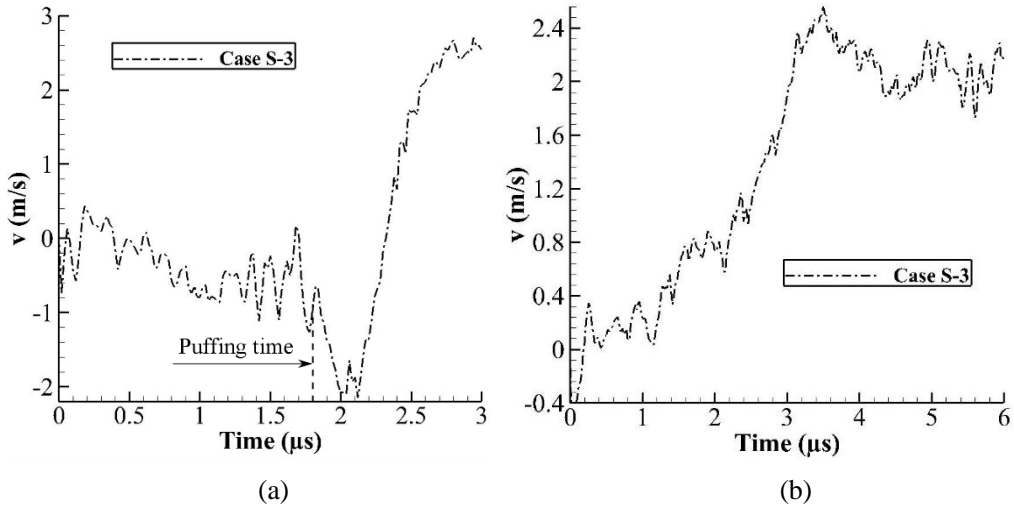
Fig. 15 Velocity traces for Case S-3. (a) The Y-direction surface velocity spatially averaged in the region defined by the white rectangle in Fig. 9c and (b) velocity of the droplet center of mass in the +Y direction.

To identify the effect of puffing on this bouncing behavior, the wall impacting Cases WI-1 to WI-4 are compared. Cases WI-1 (impact without puffing) and WI-2 (impact with puffing) are to compare the puffing effect. Cases WI-3 and WI-4 are to see the effect of the large impact inertia. Figure 16 shows the behavior of each case. It is natural that the highest Weber number cases (WI-3 and WI-4) exhibit large deformation and breakup without bouncing [58,59]. In both cases, the droplet breaks up entirely, also with rim breakup due to surface tension. This is mostly caused by the inertia of the droplet [58,59] and the effect of puffing is relatively negligible, thus these cases are not considered further.

In Cases WI-1 and WI-2, it is interesting that bouncing does not occur in WI-1 and occurs in WI-2, where the apparent impacting Weber and Reynolds numbers are the same. Generally, this small value of impacting Weber number would result in wall attachment rather than bouncing [58,59]. Therefore, this bouncing behavior is induced by the puffing effect combined. Figure 17 shows the Y-direction profiles of the surface velocity and the velocity of the center of mass for Cases WI-1 and WI-2. Puffing occurs at $t=3.2\mu s$ in Case WI-2. Until this moment, the velocities exhibit a quite similar trend of rising, which is due to mechanical repelling against the initial downward velocity. Some oscillations in WI-2 is are due to boiling bubble growth and its oscillations. Around the puffing moment at $t=3.2\mu s$ in WI-2, the surface velocity quickly rises and decreases, which indicates rupture and vapor ejection. After this, the surface and center of mass velocities largely rise in WI-2, while they do not rise over 0m/s in WI-1. This is similar to the trends shown in Fig. 15. Finally, bouncing occurs in WI-2. During puffing, the added downward surface velocity difference is around -2.5m/s (similar in Fig. 15), which effectively adds further impacting speed to the droplet.

(a) *t*=2.5μs   *t*=4.0μs   *t*=5.3μs

(b) *t*=2.5μs   *t*=3.5μs   *t*=6.9μs

(c)*t*=1.0μs   *t*=3.0μs

t=5.2μs

(d)*t*=1.0μs   *t*=3.0μs

t=5.2μs
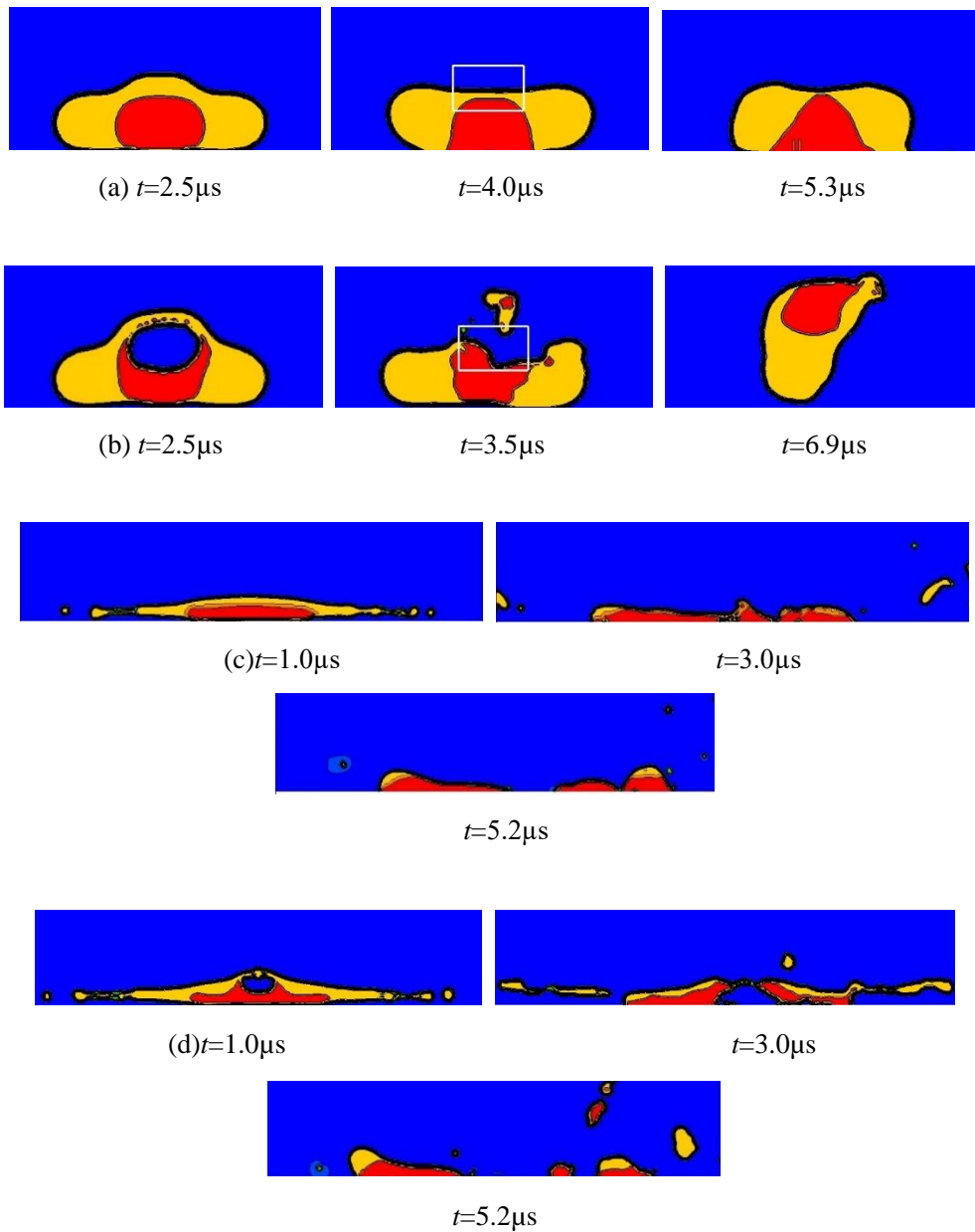
Fig. 16 Dynamics of wall impacting droplet. (a) Case WI-1, (b) Case WI-2, (c) Case WI-3 and (d) Case WI-4.
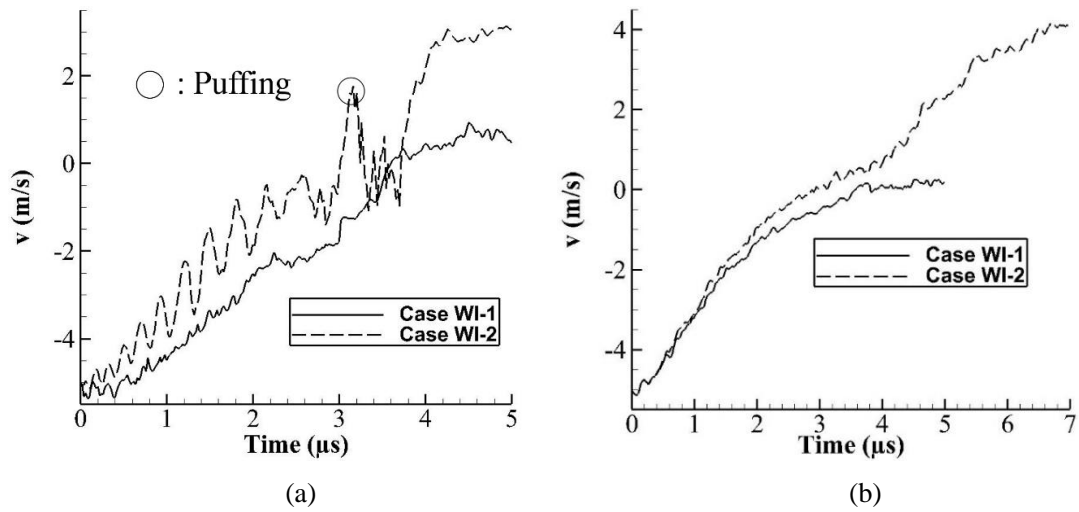
Fig. 17 Y-direction velocity profiles for wall impacting cases. (a) Surface velocity and (b) velocity of the center of mass.

The surface motion around the instant of puffing in Case WI-2 is synchronized with the droplet detaching motion. Figure 18 shows the velocity field, with the velocity vector plotted at every two grid points. When rupture occurs (Fig. 18a-b), the periphery of the ruptured hole quickly shrinks due to surface tension. Then the liquid in this region flows into the bottom side of the ejected hole (Fig. 18b-c) and this bottom part finally moves upward. This is called recoiling [17]. The recoiling motion pulls the entire droplet upward, combined with the repelling motion, and leads to wall detachment. The same behavior is observed in Case S-3, as shown in Fig. 19. Puffing adds the additional effect on impacting, and therefore, wall detachment is particularly caused.

(a) t=3.0μs

(b) t=3.3μs

(c) t=3.6μs

(d) t=3.9μs
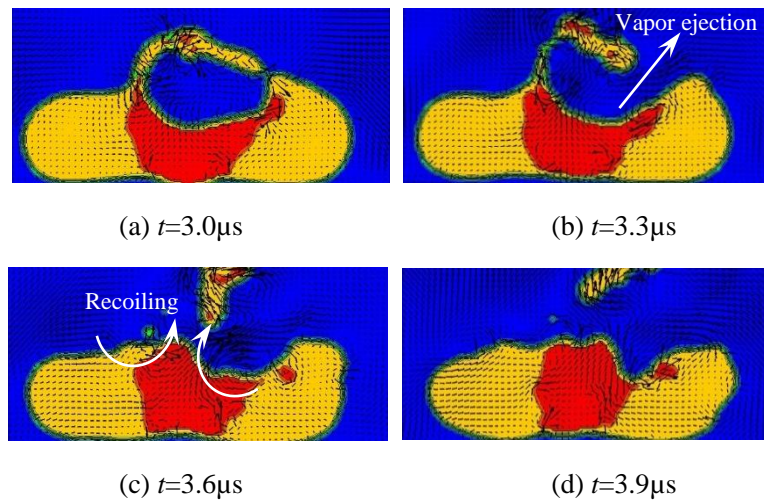
Fig. 18 Recoiling motion during puffing (Case WI-2).

20

(a) t=1.8μs   (b) t=2.0μs

(c) t=2.2μs   (d) t=2.5μs
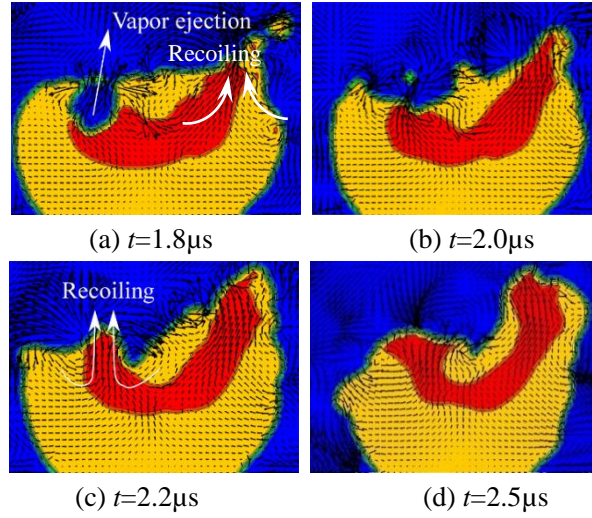
Fig. 19 Recoiling motion during puffing (Case S-3).

As seen above, the bouncing droplet dynamics is the particular characteristics of a sessile droplet with puffing. It is interesting that spray droplets once attached to the combustor wall may possibly re-join into the central part of the combustor and contribute to vapor mixing and combustion. Since the mass mixture ratio and the puffing dynamics in the present study mimic those of the realistic fuel blend [18], such a phenomenon is expected to occur in a combustor.

Finally, the degree of vapor/air mixing is discussed. In order to characterize the vapor/air mixing, the scalar dissipation rate (SDR) χ is used, which is defined as [17,20]

$$\chi = 2D_{dif}|\nabla Y_i|^2, \tag{12}$$

where D_{dif} is the diffusion coefficient. Figure 20 shows the scatter plot of the SDR of the ethanol vapor in Case F-1 (free droplet) and Case S-1 (sessile droplet) after 0.5μs from puffing. The plot is made in the direction of the vapor ejection and the dashed line represents the edge position of the primary droplet shown. The difference between Case F-1 and Case S-1 is not very much remarkable, indicating that the vapor/air mixing behavior between the free droplet and sessile droplet is similar when the puffing intensity is similarly moderate.

Next, stronger puffing cases are compared. Figure 21 shows the SDR after 0.5μs from puffing for Case F-3 (free droplet) and Case S-2 (sessile droplet). For comparison, the spatial distributions for Cases F-1 and S-1 are also plotted. For both Cases F-3 and S-2, where large breakup is caused by several bubbles, mixing is enhanced and the region of the enhanced mixing is expanded because of the effect of the stronger ethanol vapor ejection. In Fig. 21a, the distribution of the SDR for Case F-3 has several peaks. These peaks of the SDR correspond to the secondary droplet positions. Ethanol sub-droplets are fragmented into smaller secondary droplets by puffing and the remaining superheated ethanol generates vapor by boiling even outside the parent droplet, which indicates that mixing is enhanced not only by puffing but also by the continuing boiling of the secondary droplets. Therefore, if puffing (or microexplosion) positively works in a combustor, it may have a potential to unsteadily enhance vapor/air mixing and, thus improving the combustion performance. At this moment, the

puffing/microexplosion effect on vapor mixing in a turbulent spray remains unknown in a quantitative sense, and further investigation is needed in a real fuel spray. The present study may serve as a first step toward that goal.

(a-1)	(a-2)

(b-1)	(b-2)
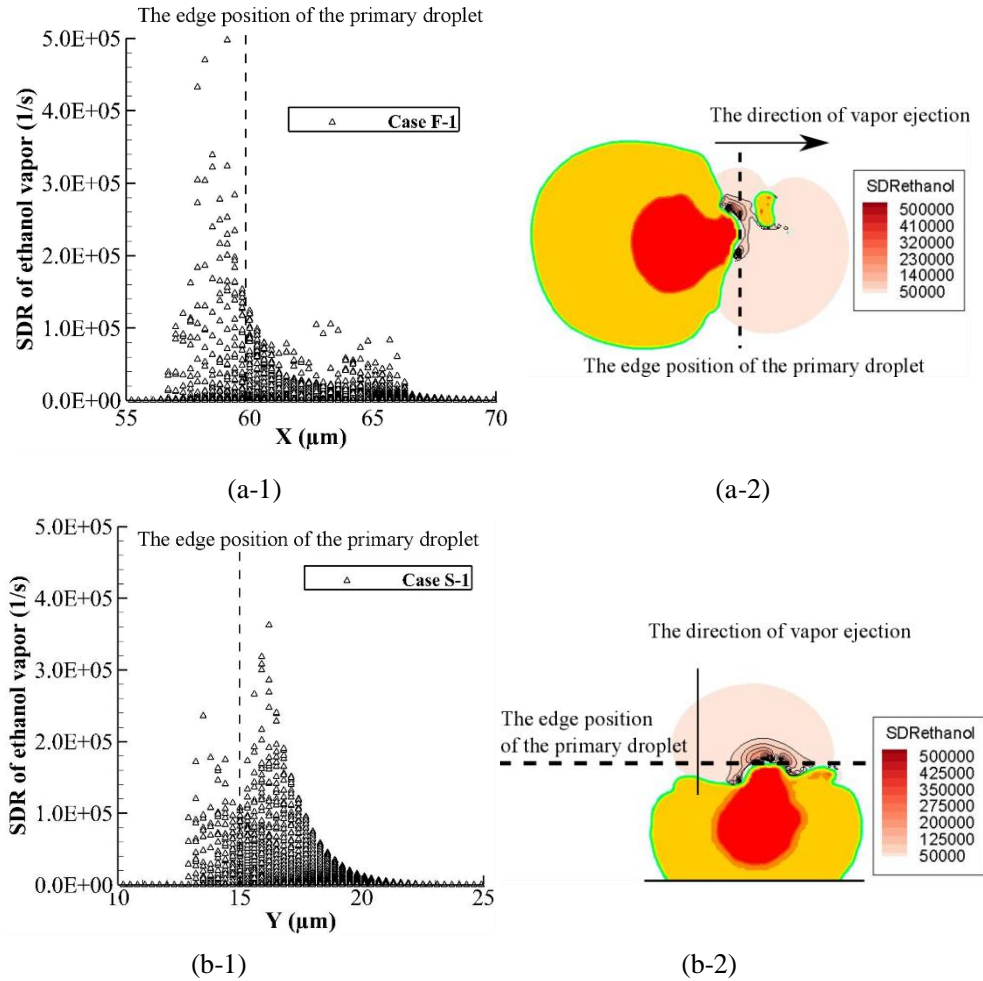
Fig. 20 The SDR of the ethanol vapor in Case F-1 at t=2.2μs and Case S-1 at t=1.7μs. (a-1) and (b-1) are scatter plots in the direction of vapor ejection and (a-2) and (b-2) show the spatial distribution.

(a-1)　　　　　　　　　　　　　　　　(a-2)

(b-1)　　　　　　　　　　　　　　　　(b-2)
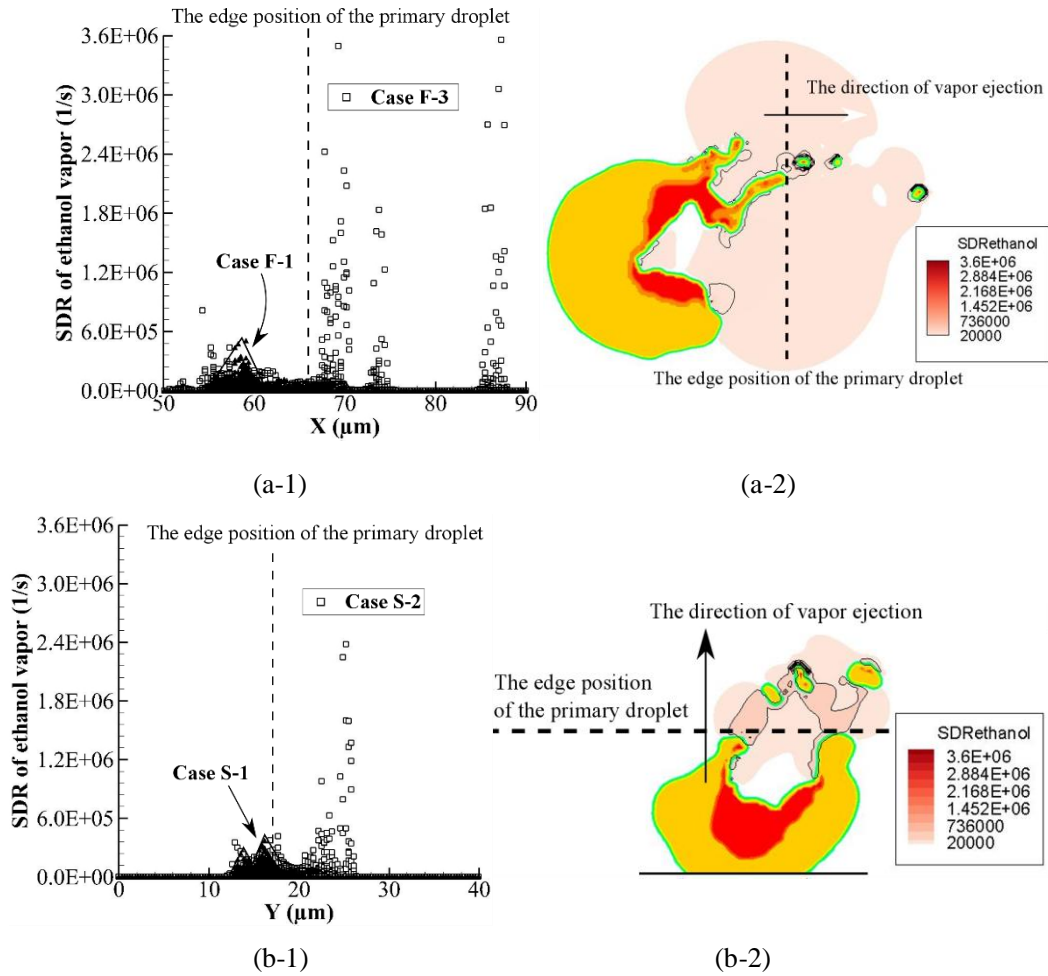
Fig. 21 The SDR of the ethanol vapor in Case F-3 at t=3.1μs and Case S-2 at t=4.5μs. (a-1) and (b-1) are scatter plots in the direction of vapor ejection and (a-2) and (b-2) show the spatial distribution.

5.　Concluding remarks

　　The secondary atomization physics by explosive boiling of emulsion fuel has been investigated for the free droplet and the sessile droplet configurations. The analysis has been conducted focusing on the behavior of bubble growth, droplet breakup and ethanol vapor mixing. The findings obtained in the present study are as follows.

(1) The number of bubbles and the bubble size just before puffing are the factors which determine the breakup degree of the droplet by puffing.

(2) The bubble size is affected by bubble coalescence or growth time. If several bubbles exist in the droplet and they are close enough to coalesce before vapor ejection, the final bubble is larger and a larger impact is caused during puffing. Even with only a single bubble, if the bubble position is deep inside the droplet, the growth time is larger and the final bubble size is larger, which causes larger breakup.

(3) If a droplet is attached to the wall, puffing may cause the droplet to detach from the wall when it

23

is strong, even if the Weber number based on the colliding velocity is small in appearance. The surface tension induced recoiling motion of the concaved surface rapidly changes the surface into convex shape and pulls the entire droplet from the wall, combined with the repelling motion. This particular dynamics, droplet bouncing and detachment from the wall, is enhanced due to puffing.

(4) The larger the degree of breakup is, the larger the local mixing becomes since the ethanol vapor ejection is stronger. Multiple ejections also affect the vapor distribution transiently. Therefore, if puffing or microexplosion is possibly used in a combustor, it may positively enhance transient mixing and thus have a potential to improve the combustion performance. At this moment, this effect of mixing enhancement in the spray scale has not been directly evaluated in a quantitative way, and further investigation is needed in the future.

References

[1] A. C. Hansen, Q. Zhang, P. W. L. Lyne, "Ethanol-diesel fuel blends - a review," *Bioresour. Technol.* 96 (2005) 277-285.

[2] A. K. Agarwal, "Biofuels (alcohols and biodiesel) applications as fuels for internal combustion," *Prog. Energy Combust. Sci.* 33 (2007) 233-271.

[3] K. Kohse-Höinghaus, P. Oßwald, T. A. Cool, T. Kasper, N. Hansen, F. Qi, C. K. Westbrook, P. R. Westmoreland, "Biofuel combustion chemistry: from ethanol to biodiesel," *Angew. Chem. Int. Ed.* 49 (2010) 3572-3597.

[4] E. Rajasekar, A. Murugesan, R. Subramanian, N. Nedunchezhian, "Review of NOx reduction technologies in CI engines fuelled with oxygenated biomass fuels," *Renew. Sust. Energy Rev.* 14 (2010) 2113-2121.

[5] S. A. Shahir, H. H. Masjuki, M. A. Kalam, A. Imran, I. M. Rizwanul Fattah, A. Sanjid, "Feasibility of diesel-biodiesel-ethanol/bioethanol blend as existing CI engine fuel: an assessment of properties, material compatibility, safety and combustion," *Renew. Sust. Energy Rev.* 32 (2014) 379-395.

[6] T. Kadota, H. Yamasaki, "Recent advances in the combustion of water fuel emulsion," *Prog. Energy Combust. Sci.* 28 (2002) 385-404.

[7] S. R. Gollahalli, M. L. Rasmussen, S. J. Moussavi, "Combustion of drops and sprays of No. 2 diesel oil and its emulsions with water," *Symp. (Int.) Combust.* 18 (1981) 349-360.

[8] J. C. Yang, G. S. Jackson, C. T. Avedisian, "Combustion of unsupported methanol/dodecanol mixture droplets at low gravity," *Symp. (Int.) Combust.* 23 (1991) 1619-1625.

[9] G. S. Jackson, C. T. Avedisian, "Combustion of unsupported water-in-n-heptane emulsion droplets in a convective-free environment," *Int. J. Heat Mass Transfer* 41 (1998) 2503-2515.

[10] D. Segawa, H. Yamasaki, T. Kadota, H. Tanaka, H. Enomoto, M. Tsue, "Water-coalescence in an oil-in-water emulsion droplet burning under microgravity," *Proc. Combust. Inst.* 28 (2000)

985-990.

[11] T. Kadota, H. Tanaka, D. Segawa, S. Nakaya, H. Yamasaki, "Microexplosion of an emulsion droplet during Leidenfrost burning," *Proc. Combust. Inst.* 31 (2007) 2125-2131.

[12] Y. Suzuki, T. Harada, H. Watanabe, M. Shoji, Y. Matsushita, H. Aoki, T. Miura, "Visualization of aggregation process of dispersed water droplets and the effect of aggregation on secondary atomization of emulsified fuel droplets," *Proc. Combust. Inst.* 33 (2011) 2063-2070.

[13] M. L. Botero, Y. Huang, D. L. Zhu, A. Molina, C. K. Law, "Synergistic combustion of droplets of ethanol, diesel and biodiesel mixtures," *Fuel* 94 (2012) 342-347.

[14] K. L. Pan, M. C. Chiu, "Droplet combustion of blended fuels with alcohol and biodiesel/diesel in microgravity condition," *Fuel* 113 (2013) 757-765.

[15] S. Moon, T. Tsujimura, M. Oguma, Z. Chen, Z. Huang. T. Saitou, "Mixture condition, combustion and sooting characteristics of ethanol-diesel blends in diffusion flames under various injection and ambient conditions," *Fuel* 113 (2013) 128-139.

[16] J. Shinjo, J. Xia, L. C. Ganippa, A. Megaritis, "Physics of puffing and microexplosion of emulsion fuel droplets," *Phys. Fluids* 26 (2014) 1-22.

[17] J. Shinjo, J. Xia, L. C. Ganippa, A. Megaritis, "Puffing-enhanced fuel/air mixing of an evaporating *n*-decane/ethanol emulsion droplet and a droplet group under convective heating," *J. Fluid Mech.* 793 (2016) 444-476.

[18] M. M. Avulapati, L. C. Ganippa, J. Xia, A. Megaritis, "Puffing and micro-explosion of diesel-biodiesel-ethanol blends," *Fuel* 166 (2016) 59-66.

[19] Y. Zhang, R. Huang, Z. Wang, S. Xu, S. Huang, Y. Ma, "Experimental study on puffing characteristics of biodiesel-butanol droplet," *Fuel* 191 (2017) 454-462.

[20] J. Shinjo, J. Xia, "Combustion characteristics of a single decane/ethanol emulsion droplet and a droplet group under puffing conditions," *Proc. Combust. Inst.* 36 (2017) 2513-2521.

[21] D. C. K. Rao, S. Karmakar, S. Basu, "Atomoization characteristics and instabilities in the combustion of multi-component fuel droplets with high volatility differential," *Sci. Rep.* 7 (2017) 1-15.

[22] P. Satgé de Caro, Z. Mouloungui, G. Vaitilingom, J. Ch. Berge, "Interest of combining an additive with diesel-ethanol blends for use in diesel engines," *Fuel* 80 (2001) 565-574.

[23] D. B. Hulwan, S. V. Joshi, "Performance, emission and combustion characteristic of a multicylinder DI diesel engine running on diesel-ethanol-biodiesel blends of high ethanol content," *Appl. Energy* 88 (2011) 5042-5055.

[24] L. Pidol, B. Lecointe, L. Starck, N. Jeuland, "Ethanol-biodiesel-diesel fuel blends: performance and emissions in conventional diesel and advanced low temperature combustions," *Fuel* 93 (2012) 329-338.

[25] H. Watanabe, K. Okazaki, "Visualization of secondary atomization in emulsified-fuel spray flow by shadow imaging," *Proc. Combust. Inst.* 34 (2013) 1651-1658.

[26] H. Liu, C. Lee, M. Huo, M. Yao, "Comparison of ethanol and butanol as additives in soybean biodiesel using a constant volume combustion chamber," *Energy Fuels* 25 (2011) 1837-1846.

[27] R. Ochoterena, A. Lif, M. Nydén, S. Andersson, I. Denbratt, "Optical studies of spray

development and combustion of water-in-diesel emulsion and microemulsion fuels," *Fuel* 89 (2010) 122-132.

[28] M. Huo, S. Lin, H. Liu, C. F. Lee, "Study on the spray and combustion characteristics of water-emulsified diesel," *Fuel* 123 (2014) 218-229.

[29] C. T. Avedisian, R. P. Andres, "Bubble nucleation in superheated liquid–liquid emulsions," *J. Colloid Interface Sci.* 64 (1978) 438-453.

[30] C. T. Avedisian, "Superheating and boiling of water in hydrocarbons at high pressures," *Int. J. Heat Mass Transfer* 24 (1981) 695-706.

[31] C. T. Avedisian, "The homogeneous nucleation limits of liquids," *J. Phys. Chem. Ref. DatS-1*4 (1981) 695-729.

[32] C. T. Avedisian, J. R. Sullivan, "A generalized corresponding states method for predicting the limits of superheat of mixtures," *Chem. Eng. Sci.* 39 (1984) 1033-1041.

[33] N. Miyamoto, H. Ogawa, M. Nabi, "Approaches to extremely low emissions and efficient diesel combustion with oxygenated fuels," *Int. J. Engine Res.* 1 (2000) 71-85.

[34] S. Sakai, D. Rothamer, "Effect of ethanol blending on particulate formation from premixed combustion in spark-ignition engines," *Fuel* 196 (2017) 154-168.

[35] M. Mikami, N. Kojima, "An experimental and modeling study on stochastic aspects of microexplosion of binary-fuel droplets," *Proc. Combust. Inst.* 29 (2002) 551-559.

[36] J. Shinjo, J. Xia, A. Megaritis, L. C. Ganippa, R. F. Cracknell, "Modeling temperature distribution inside and emulsion droplet under convective heating: a key to predicting microexplosion and puffing," *Atom. Sprays* 26 (2016) 551-583.

[37] J. Shinjo, A. Umemura, "Fluid dynamic and autoignition characteristics of early fuel sprays using hybrid atomization LES," *Combust. Flame* 203 (2019) 313-333.

[38] M. Sussman, P. Smereka, S. Osher, "A level set approach for computing solutions to incompressible two-phase flow," *J. Comput. Phys.* 114 (1994) 146-159.

[39] S. Tanguy, T. Menard, A. Berlemont, "A level set method for vaporizing two-phase flows," *J. Comput. Phys.* 221 (2007) 837-853.

[40] J. U. Brackbill, D. B. Kothe, C. Zemach, "A continuum method for modeling surface tension," *J. Comput. Phys.* 100 (1992) 335-354.

[41] T. Kunugi, "Direct numerical algorithm for multiphase flow with free surfaces and interfaces," *J. Jpn. Soc. Mech. Eng. B* 63. (1997) 1576-1584

[42] M. Sussman, E. G. Puckett, "A coupled level set and volume-of-fluid method for computing 3D and axisymmetric incompressible two-phase flows," *J. Comput. Phys.* 162 (2000) 301-337.

[43] J. Shinjo, A. Umemura, "Simulation of liquid jet primary breakup: dynamics of ligament and droplet formation," *Int. J. Multiphase Flow* 36 (2010) 513-532.

[44] J. Shinjo, A. Umemura, "Detailed simulation of primary atomization mechanisms in diesel jet sprays (isolated identification of liquid jet tip effects)," *Proc. Combust. Inst.* 33 (2011) 2089-2097.

[45] J. Shinjo, A. Umemura, "Droplet/turbulence interaction and early flame kernel development in an autoigniting realistic dense spray," *Proc. Combust. Inst.* 34 (2013) 1553-1560.

[46] H. Takewaki, A. Nishiguchi, T. Yabe, "Cubic interpolated pseudo-particle method (CIP) for solving hyperbolic-type equations," *J. Comput. Phys.* 61 (1985) 261-268.

[47] T. Yabe, F. Xiao, T. Utsumi, "The constrained interpolation profile method for multiphase analysis," *J. Comput. Phys.* 169 (2001) 556-593.

[48] O. A. Basaran, "Nonlinear oscillations of viscous liquid drops," *J. Fluid Mech.* 241 (1992) 169-198.

[49] M. S. Plesset, S. A. Zwick, "The growth of vapor bubbles in superheated liquids," *J. Appl. Phys.* 25 (1954) 493-500.

[50] B. B. Mikic, W. M. Rohsenow, P. Griffith, "On bubble growth rates," *Int. J. Heat Mass Trans.* 13 (1970) 657-666.

[51] C. E. Brennen, *Cavitation and Bubble Dynamics*, Oxford Univ. Press, Oxford, 1995.

[52] A. Umemura, Y. Shimada, Characteristics of supercritical droplet gasification, *Symp. (Int.) Combust.* 26 (1996) 1621-1628.

[53] NIST (National Institute of Standards and Technology) Chemistry WebBook, retrieved in Apr. 2014 from http://webbook.nist.gov/chemistry/fluid/

[54] M. Gao, P. Kong, L. Zhang, "Evaporation dynamics of different sizes sessile droplets on hydrophilic and hydrophobic heating surface under constant wall heat fluxes conditions," *Int. J. Heat Mass Transfer* 93 (2018) 93-99.

[55] Deendarlianto, Y. Takata, S. Hidaka, Indarto, A. Widyaparaga, S. Kamal, Purnomo, M. Kohno, "Effect of static contact angle on the droplet dynamics during the evaporation of a water droplet on the hot walls," *Int. J. Heat Mass Transfer* 71 (2014) 691-705.

[56] F. Liu, N. Kang, Y. Li, Q. Wu, "Experimental investigation on the spray characteristics of a droplet under sinusoidal inertial force," *Fuel* 226 (2018) 156-162.

[57] F. Liu, N. Kang, Y. Li, Q. Wu, "Experimental investigation on the atomization of a spherical droplet induced by Faraday instability," *Exp. Therm. Fluid Sci.* 100 (2019) 311-318.

[58] S. Wildeman, C. W. Visser, C. Sun, D. Lohse, "On the spreading of impacting drops," *J. Fluid Mech.* 805 (2016) 636-655.

[59] I. V. Roisman, J. Breitenbach, C. Tropea, "Thermal atomisation of a liquid drop after impact onto a hot substrate," *J. Fluid Mech.* 842 (2018) 87-101.